Volume 1 Issue 1 (September 2021)
DOI 10.24191/jaeds.v1i1.31
eISSN 2805-5756

Journal of Applied Engineering Design & Simulation

# Methodical Procedure of Virtual Manufacturing for Analysing WAAM Distortion along with Experimental Verification

K.P Prajadhiana[1], Y.H.P Manurung[1*], M.A Mohamed[2] and A. Bauer[3]
[1]Smart Manufacturing Research Institute, Universiti Teknologi MARA, Shah Alam 40450 Selangor, Malaysia.
[2]Serba Dinamik Group Berhad, Shah Alam 40000 Selangor, Malaysia.
[3] Professorship of Virtual Production Engineering, Chemnitz University of Technology, Chemnitz 9130 Sachsen, Germany.
[*]corresponding author: yupiter.manurung@uitm.edu.my

## ABSTRACT

This paper deals with an initial development of virtual manufacturing (VM) procedure to predict substrate distortion induced by Wire Arc Additive Manufacturing (WAAM) process. In this procedure, a hollow shape is designed in a thin-walled form made of stainless steel. The procedure starts with geometrical modelling of WAAM component consisting of twenty-five deposited layers with austenitic stainless-steel wire SS316L as feedstock and SS304 as substrate material. The hollow shape is modelled based on simplified rectangular mesh geometry with identical specimen dimensions during the experiment. Material model to be defined can be retrieved directly from a database or by conducting a basic experiment to obtain the evolution of material composition, characterized using Scanning Electron Microscopy (SEM) with Energy Dispersive X-ray (EDX) analysis, and generated using advanced modelling software JMATPRO for creating new properties including the flow curves. Further, a coupled thermomechanical solution is adopted, including phase-change phenomena defined in latent heat, whereby temperature history due to successive layer deposition is simulated by coupling the heat transfer and mechanical analysis. Transient thermal distribution is calibrated from an experiment obtained from thermocouple analysis at two reference measurement locations. New heat transfer coefficients are to be adjusted to reflect actual temperature change. As the following procedure prior to simulation execution, a sensitivity analysis was conducted to find the optimal number of elements or mesh size towards temperature distribution. The last procedure executes the thermomechanical numerical simulation and analysis the post-processing results. Based on all aspects in VM procedures and boundary conditions, WAAM distortion is verified by means of experimental WAAM process using a robotic welding system equipped with a pulsed power source. The experimental substrate distortion is measured at various points before and after the process. It can be concluded based on the adjusted model and experimental verification that using nonlinear numerical computation, the prediction of substrate distortion with evolved material property of component yields closer average result within the relative error less than 11% compared to database material giving doubled inaccuracy up to 22%.

**Keywords**: virtual manufacturing, WAAM, distortion, material modelling, experiment

***Nomenclature (Greek symbols towards the end)***

| | |
|---|---|
| *A* | Current of the WAAM process |
| *Mm/s* | Speed of WAAM Deposition |
| *Mm/min* | Wire Feed-rate |
| *V* | Voltage within WAAM process |

***Abbreviations***

| | |
|---|---|
| AM | Additive Manufacturing |
| FEM | Finite Element Method |
| GMAW | Gas Metal Arc Welding |
| VM | Virtual Manufacturing |
| WAAM | Wire-Arc Additive Manufacturing |

Received on 02.09.2021
Accepted on 20.09.2021
Published on 05.10.2021

## 1.0 INTRODUCTION

Finite Element (FE) - based Virtual Manufacturing (VM) is increasingly implemented to tackle the prediction challenges faced in modern engineering due to increasing demands in manufacturing time and product quality. VM can be seen as one of the crucial components within Virtual Engineering in which a realization of a real manufacturing process can utilize the numerical computation. The VM's primary function is to model the entire manufacturing process to enhance decision-making and quality control within the manufacturing process [1-2]. Numerical computation is divided into several sub-technologies, which are still evolving up until today. The simulation that investigates a product's life cycle by means of VM is based on numerical computation, which covers all activities and functions from drafting to prototyping [3].

Today's businesses continually search for ways to increase productivity in product development [4]. This can be done using virtual prototypes that can be easily duplicated and shared between everyone involved. In addition to this product design process, the stability of the manufacturing process and the resulting product quality ultimately determine the product's profitability. The manufacturing concepts of a new product use the systems that integrate computer models that represent precisely the whole structure of the manufacturing process and simulate their physical and logical behavior in operation [5]. Virtual engineering (VE) technologies play a significant role in integrating the computer-based technologies involved in the product's life cycle, accompanied by reliable data transfer to the circle of computer-based technologies [6].

In recent years, Additive Manufacturing (AM) has been used to produce a build-up product by means of layer-by-layer deposition instead of employing the traditional machining of raw materials. Some of the most popular techniques developed for manufacturing metal structures in AM are laser sintering, direct metal deposition, electron beam melting, shape deposition manufacturing, and wire arc additive manufacturing (WAAM) [7]. In WAAM, a filler material is usually melted using an electric arc which is established between the consumable wire electrode and the top surface of deposited layers [8]. The component formed by depositions experiences the heating and cooling with a moving heat source model.

The involvement of FE-based VM in investigating the WAAM processes for both thermal and mechanical aspects has been an interest of research within engineering environment in recent years. Many engineering studies have been conducted to evaluate the effect of interposed temperature within WAAM specimen. The engineering research which concerns about the usage of FE analysis on WAAM investigation showed that the high deposition rate of process allows the creation of complex metal components in a flexible manner with high velocity. However, at some cases, such flexibility results in large thermal gradients in the work piece which can cause the emergence of distortion [9-11].

A comprehensive procedure of FE-based VM could assist in the prediction of distortion induced by WAAM process with small error percentage when both numerical simulation results are compared [12]. WAAM research is conducted focusing on thermo-mechanical modelling by utilizing commercial-based VM software for semi-finished product, and the research leads to a conclusion that the orientation position of bead deposition and component geometry exhibits critical influence on temperature distribution [13]. Another research was performed by Yehorov et al. on the process control towards the WAAM deformation which defined that the usage of numerical computation is able to reduce the porosity within the final product of WAAM component due to the optimized parameters [14-15]. Further research used advanced numerical computation via FE modelling to investigate the distortion induced by a WAAM process as well as the effects of cooling conditions applied in the deposition of the different layers [16-17].

The usage of stainless steel SS316L in additive manufacturing process has been performed in many engineering researches. An advanced research focusing on both temperature and residual stresses induced by multi-pass of welding stainless steel (state material) was conducted with the final results showing the correlation between temperature distribution and residual stresses; thus, this research shared a similar basic concept with WAAM process [18]. Several mechanical property investigations which involved stainless steel SS316L as the feedstock in AM process were carried out and the researcher found that stainless steel SS316L possesses high mechanical values such as yield strength while maintaining a good ductility and notch impact resistance, which is suitable for AM-related processes [19-20]. Another advanced engineering research found that SS316L is suitable as feedstock in AM process as well as for the WAAM technology because the material possesses high strength, high ductility as well as excellent corrosion resistance [21-22].

Based on past research, there were less attempts carried out on substrate distortion of distinct component shape such as hollow form. Since the behaviour of temperature distribution as well as the deformation is unknown, a detailed investigation should be conducted to understand the deformation of the component. In this research, a hollow rectangular shape of twenty-five layers along with its substrate is to be studied using pulsed WAAM process. Two material models were selected for WAAM component based on the database provided by VM software as well as evolved component properties examined after the layer depositions using the SEM/EDX for a commercial SS316L filler material. The substrate of the base plate is made of stainless steel SS304, the material model which is taken from software database is to be analysed with regard to the total deformation after the

WAAM process. The basic procedures of VM for WAAM research is shown in Fig. 1 as proposed by author's previous research [23].

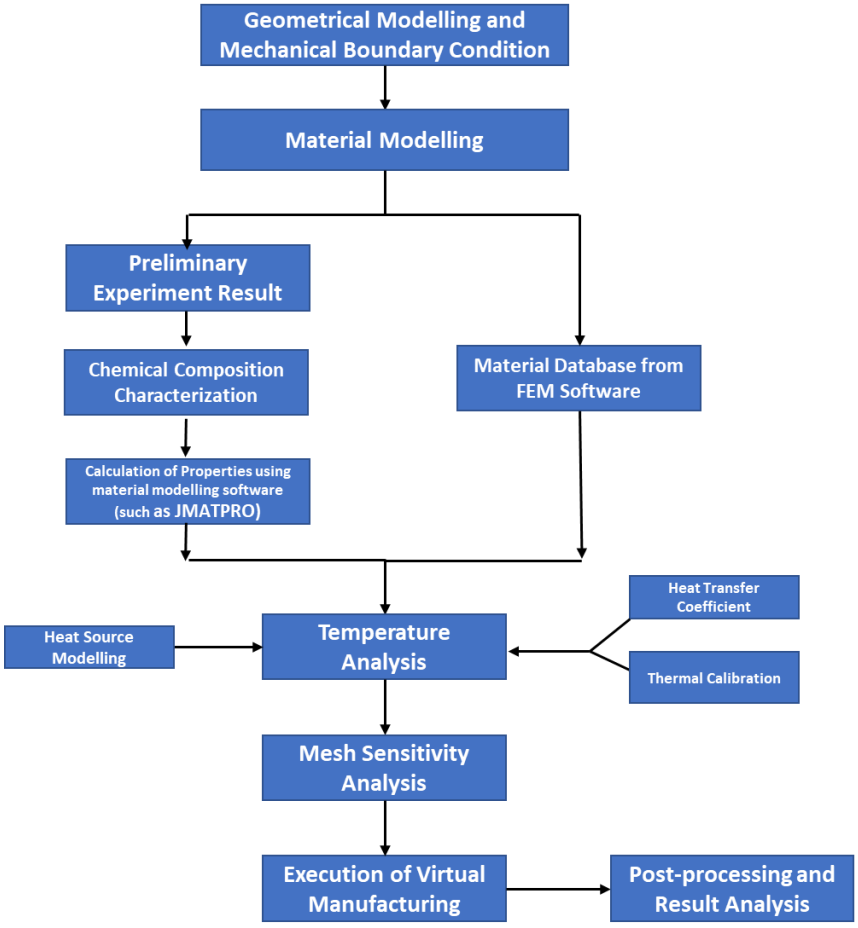


**Figure 1.** Methodical VM procedure of WAAM research on distortion

## 2.0 THERMOMECHANICAL VIRTUAL MANUFACTURING SET-UP AND PROCEDURE

In the modelling and simulation of hollow-shaped WAAM processes, sequentially coupled transient thermomechanical FE analysis using MSC Marc/Mentat was executed. Thereby, the component material was modelled based on evolved chemical composition and from software database. The process was simulated by means of birth-and-death element method. The heat source model for GMAW process was selected under consideration of heat losses which was further investigated using thermal calibration between experiment and simulation. Other conditions such as clamping position were also modelled based on actual location in experiment.

### 2.1 VM procedure for geometrical modelling and boundary condition

The geometrical modelling for this WAAM model was based on a thin-walled plate along with a wall of the WAAM component developed by the beads. The substrate plate had the dimension of 140 mm (L) x 60 mm (W) x 4 mm (T) which was made of stainless steel SS304 plate similar to the experiment. This rectangular-shaped model with 105 mm in length, 25 mm in width and 37.5 mm in height was modelled as component with a similar height of every layer. This simplified bead model was proven to produce good results as discussed in previous research [24]. While meshing 25 layers, each layer zone was discretized by means of 224 hexahedral elements in a uniform mesh thickness of 1.5 mm. The basic FE model with simplified bead modelling for this multi-layer WAAM and the clamping condition is shown in Fig. 2.

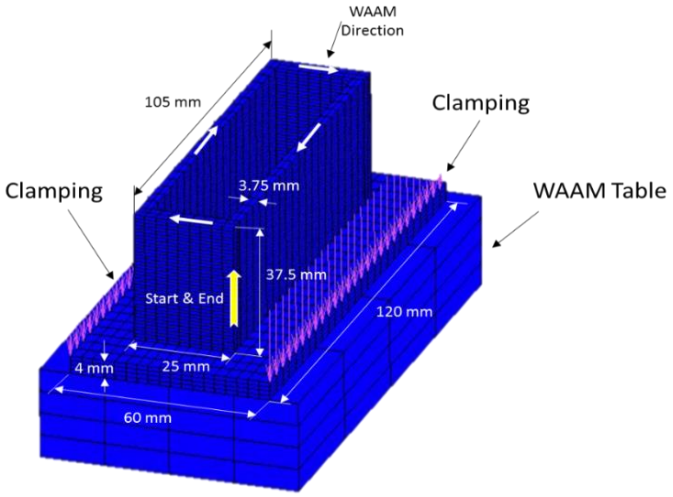


**Figure 2.** Detailed configuration for numerical model of WAAM simulation

## 2.2 VM procedure for material modelling

### 2.2.1 Preliminary experiment for determining material property

The rectangular hollow shape was built using a series of WAAM deposition using robotic welding system with a stainless steel SS316L filler wire (diameter = 1.2 mm). For the substrate, a commercially available stainless-steel plate (SS304) with a dimension of 140 mm (L) x 60 mm (W) x 4 mm (t) was used. The deposition consisted of 25 layers of beads in aforementioned shape on top of the rectangular substrate. For the experiments, the apparatus comprised of a robotic welding system ABB IRB 2400/16 and an inverter power source KEMMPI Pro Evolution ProMIG 540MXE. The trajectory of WAAM feedstock was executed by means of Pulse Welding with a dimension of 100 mm (L) x 20 mm (W) for 25-layers. Fig. 3 displays both robotic welding equipment as well as the final WAAM component with a dimension of avg. 105 mm (L) x avg. 25 mm (W) x avg. 37.5 mm (h) and a wall thickness of avg. 3.75 mm.

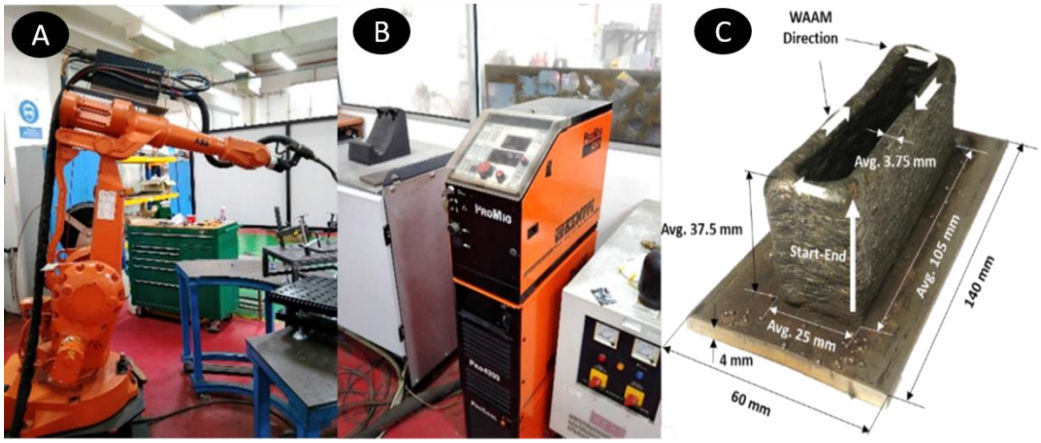


**Figure 3.** Robotic welding equipment (A), weld power source (B) and final WAAM component (C)

Due to a similar base concept with multi-layered GMAW, parameters which are common to be found in GMAW processes such as potential, arc current, welding and wire feed speed were selected according to the quality level of deposited weld beads. The current was set based on the principle of a pulsed GMAW process which constantly switched between high (peak) amperage to low (background) amperage. This configuration was regulated within a KEMPPI synergic welding power source which provided uniform current pulses to detach identical molten droplets of predetermined volume from the electrode wire, combined with the other parametric relationships necessary for a stable wire burn-off. The three essential characteristics of synergic pulse welding operations are automatically selected pulse parameters, direct relation of pulse frequency to wire feed rate and uniform weld bead profile as well as penetration through an electronic parameter control. Table 1 lists the parameters selected for the WAAM experiment.

**Table 1:** Experimental parameters and results using robotic system with GMAW-P

| Experimental Parameters | Value |
|---|---|
| Base Current [A] | 88 – 110 |
| Peak Current [A] | 275 - 300 |
| Voltage [V] | 21 |
| Welding speed [mm/s] | 7 |
| Wire feed rate [m/min] | 3 |
| Gas composition [%] | 100% Argon |
| Number of Layers [-] | 25 |
| Height of Component [mm] | Avg. 37.5 |
| Width of Component [mm] | Avg. 25 |
| Thickness of Component [mm] | Avg. 3.75 |

The calibration method for the simulation of WAAM process was verified by means of temperature distribution comparison analysis. For measuring the temperature distribution, a data logger (ALMEMO 2890-9) and thermocouples (type K) were used, arranged onto the specimen as shown in Fig. 3. The thermocouple type-K was chosen due to the ability to measure high temperatures up to 1370 °C. To analyse the temperature level, the thermocouples were inserted into the substrate of the specimen immediately after the wire deposition at location 2. In the filler deposition, although the drilled thermocouple might melt at the tip along with the molten portion of filler, the rest of the thermocouple remained and was able to capture the actual temperature. The recording time of the thermocouple generated by the system was executed once the filler material started to solidify. Fig. 4 shows the temperature distribution of 25 layers of WAAM on two selected locations in the bead and at the 11$^{th}$ layer deposition. The distortion measured by the use of a Mitutoyo Beyond 707 Coordinate Measuring Machine (CMM) was chosen as validation method executed on the base plate of the specimen before and after the experimental process.

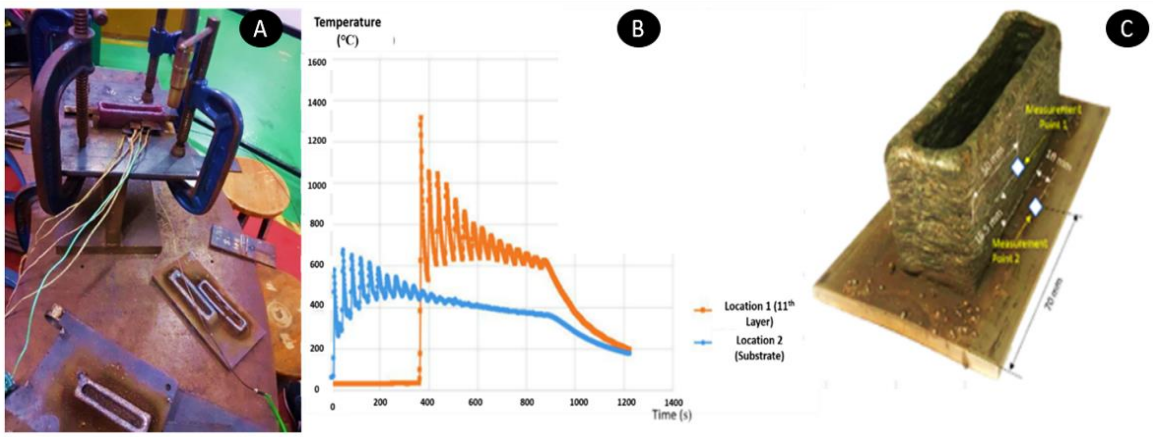


**Figure 4.** Experimental setup (left), temperature distribution measurement (middle) and a close up of WAAM component (right)

The experimental SS316L was analysed by using SEM-EDX (Hi-Tech Instrument SU3500) machine in order to extract the chemical composition data that would be later be implemented in FE analysis. Fig. 5 shows the specimen sample and results using SEM/EDX. The chemical compositions obtained from component material, which was the evolved SS316L component and software database, can be seen in Table 2.

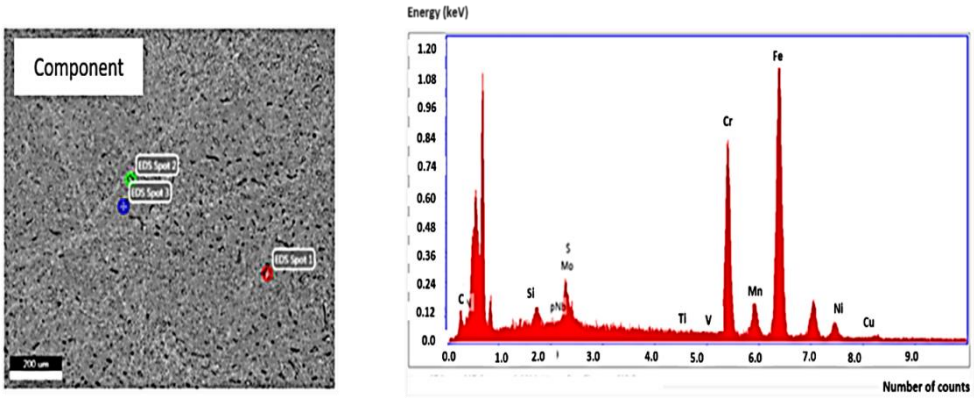


**Figure 5.** Results of chemical composition of evolved component using SEM-EDX

**Table 2**: Chemical compositions of evolved component, database of SS316 and substrate SS304

| Material | C | Cu | Cr | Mn | Mo | N | Ni | S | Si | Ti | V | P |
|---|---|---|---|---|---|---|---|---|---|---|---|---|
| Evolved Component | 0.03 | 0.76 | 17.83 | 2.43 | 1.63 | N/A | 10.57 | N/A | 0.63 | 0.267 | 0.3 | N/A |
| Software Database (SS316L) | 0.018 | N/A | 16.63 | 1.57 | 2.05 | 0.00153 | 11.18 | 0.48 | 0.002 | N/A | N/A | 0.04 |
| Software Database (SS304) | 0.08 | N/A | 20 | 2 | N/A | 0.1 | 10.5 | 0.03 | 0.75 | N/A | N/A | 0.45 |

### 2.2.2 Material property modelling of SS316L

This simulation assigned a stainless-steel type of material for both filler and substrate material. SS316L was chosen as filler material and SS304 as the substrate. The material modelling data for the substrate was obtained from the software database, while the data for the component was developed from actual WAAM-deposited SS316L material. The method of extracting the real material data using EDX for the development of VM simulation was performed for AM [25]. The experimental SS316L was analysed by using SEM-EDX (Hi-Tech Instrument SU3500) to extract the chemical composition data that would be later implemented in the FE analysis with the material modelling feature given by MSC Marc/Mentat. The new temperature-dependant physical properties of the component material were generated which covered thermal conductivity, expansion coefficient, specific heat capacity and Young's modulus. Fig. 6 displays the temperature-dependant properties of SS316L and Fig. 7 shows the flow curve at the strain rate of 0.001 $sec^{-1}$ generated with the material modelling software JMATPRO [26].

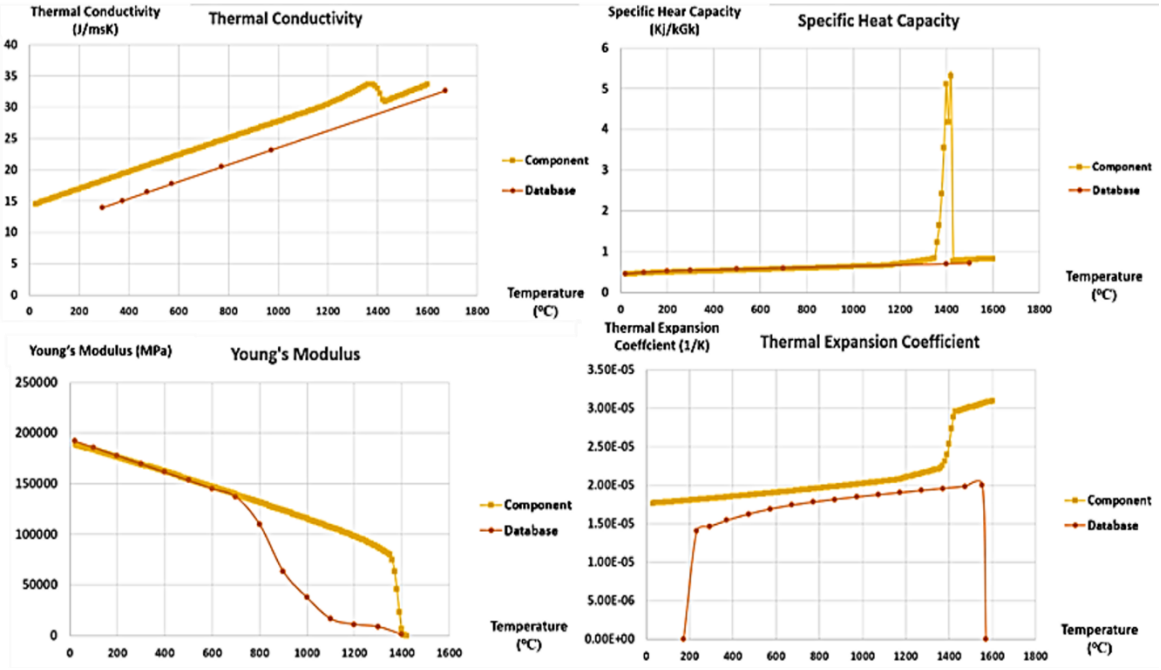


**Figure 6.** Evolved material properties of component based on EDX result and JMATPRO

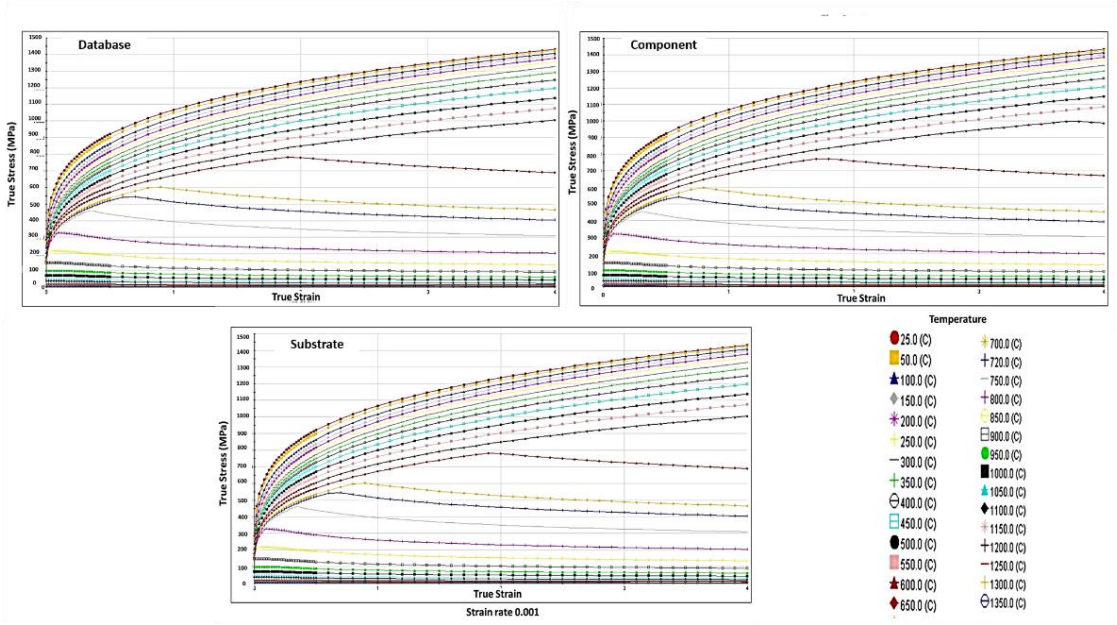


**Figure 7.** Flow curve of database, evolved component material of SS316L and Substrate SS304 at strain rate 0.001 $sec^{-1}$

### 2.3 VM procedure for heat source modelling

In WAAM modelling and simulation, process parameters assigned within the model were Current (I), Voltage (V) and travel speed (v), latent heat (256400 J/kg), solidus (1279 °C) and liquidus (1430 °C) temperature as defined according to SS316L material database values. The parameters were similar for both VM simulations with different materials. Table 3 displays the WAAM process parameters in MSC Marc/Mentat.

**Table 3:** WAAM parameters used in MSC Marc simulation

| WAAM Parameter | Value |
|---|---|
| Current [A] | 88 |
| Voltage [V] | 21 |
| Travel speed [mm/s] | 7 |

The heat source model of Goldak's double ellipsoid defines the heat source dimension [27]. The heat source models represent the state of art in WAAM simulations in which the concept evolved from multi-layered welding. This model has also a function to generate the amount of heat while at the same time it is able to control the overall power poured into both substrate and weld deposits. In this model, the heat input is delivered over a moving double ellipsoid region according to Gaussian distribution [28]. Despite such strategy permits to correctly model the shape of the weld pool, it does not take into account the correct heat distribution between filler and base material. Fig. 8 displays Goldak's double ellipsoid heat source model along with its explanation.

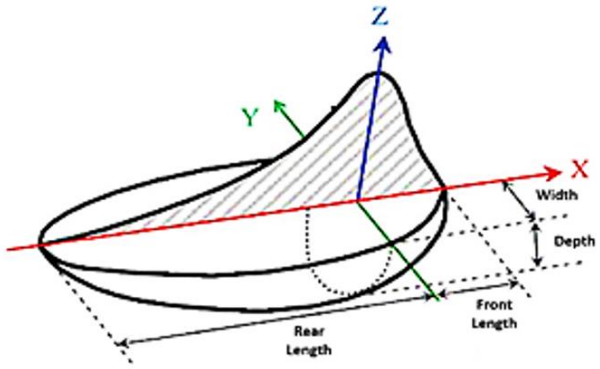


**Figure 8**. Illustration of Goldak's Double Ellipsoid Heat Source Model [29]

The values for each direction used in WAAM simulation are shown in Table 4. The dimensions differ depending on the size of the weld bead or thermal distribution.

**Table 4:** Heat Source Dimension in WAAM Simulation

| Heat Source dimensions | Value |
|---|---|
| Width b (mm) | 5 |
| Depth c (mm) | 5 |
| Front Length $a_f$ (mm) | 3 |
| Rear Length $a_r$ (mm) | 6 |

The power density distribution of the moving heat source model is described in Eq. 1, where $a_f$, $a_r$, b and c are the semi axis of the ellipsoid. The fractions of deposited head $f_f$ and $f_r$ represent the heat apportionments of the heat flux in the front and rear quadrants, provided that the condition $f_f + f_r = 2$ is fulfilled.

$$q_f(x,y,z) = \frac{6\sqrt{3}Qf_f}{a_f bc\pi\sqrt{\pi}} \exp\left(-\frac{3x^2}{a_f^2} - \frac{3y^2}{b^2} - \frac{3z^2}{c^2}\right) \quad (1)$$

$$q_r(x,y,z) = \frac{6\sqrt{3}Qf_r}{a_f bc\pi\sqrt{\pi}} \exp\left(-\frac{3x^2}{a_r^2} - \frac{3y^2}{b^2} - \frac{3z^2}{c^2}\right) \quad (2)$$

### 2.4 VM Procedure for Thermal Calibration

The calibration method of this study was examined by analysing the comparison of transient temperature distribution between WAAM simulation and experiment. This calibration method has been utilized by numerous

researchers in similar areas in order to ensure the optimization of thermal parameters in their simulation [30-32]. The usage of thermal distribution on WAAM processes was also executed by comparing experimental and simulation of WAAM [33]. Fig. 9 displays the temperature distribution comparison result on two different measurement points. The comparison of the temperature distribution was taken within the substrate as well as the 11$^{th}$ layer of the filler wire deposition.

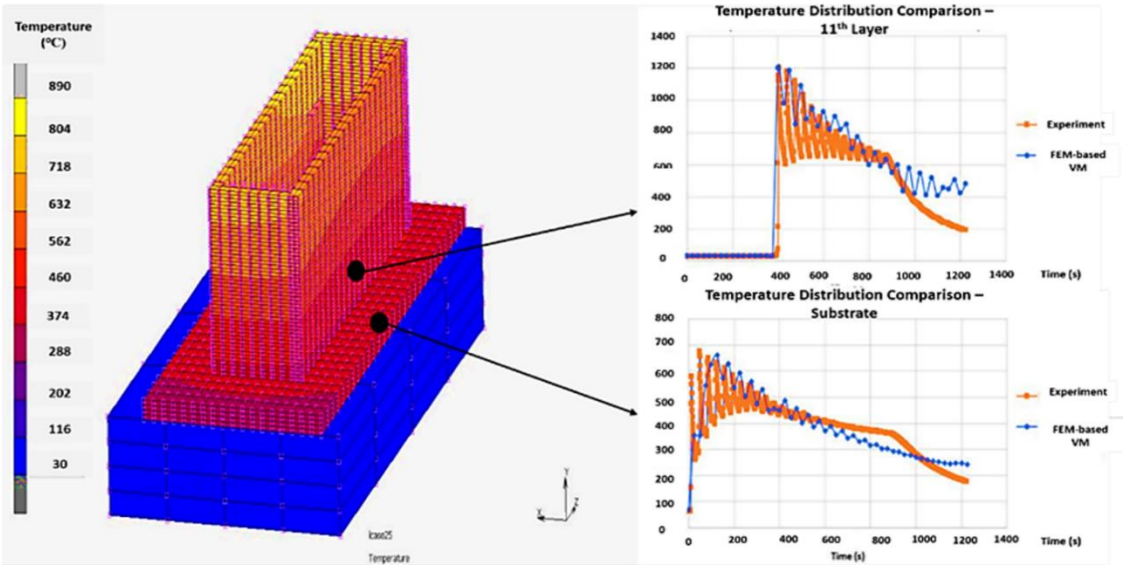


**Figure 9.** Comparison of experimental and VM-based temperature distribution at similar location

Based on the temperature distribution comparison, it was observed that the temperature behaviour between WAAM simulation and experiment shared a similar pattern. The adjusted heat transfer coefficients for the WAAM simulation model using MSC Marc/Mentat are displayed in Table 5.

**Table 5:** Adjusted heat transfer coefficients used in VM procedure

| Numerical Parameters | Value |
|---|---|
| Heat Transfer Coefficient, Metal to Metal [W/m$^2$/K] | 2500 |
| Heat Transfer Coefficient, Metal to Environment [W/m$^2$/K] | 25 |
| Initial Temperature [°C] | 30 |

### 2.5 VM procedure for analysing optimal mesh size

Before the execution of numerical computation using FE analysis, a mesh sensitivity analysis was conducted in order to determine the suitable mesh size to be implemented for the whole research. The other purpose of executing the mesh sensitivity analysis for this research was to find a trade-off between solution reliability and computational time. Mesh sensitivity study is a simple way to check potential singularity points in the mesh [34].

The numerical simulation of WAAM processes in this particular study was only developed in two layers to simplify the mechanism of mesh sensitivity analysis and to reduce the overall computational time. The geometrical design of WAAM component which serves as the basis of this sensitivity analysis is displayed in Fig. 10 below.

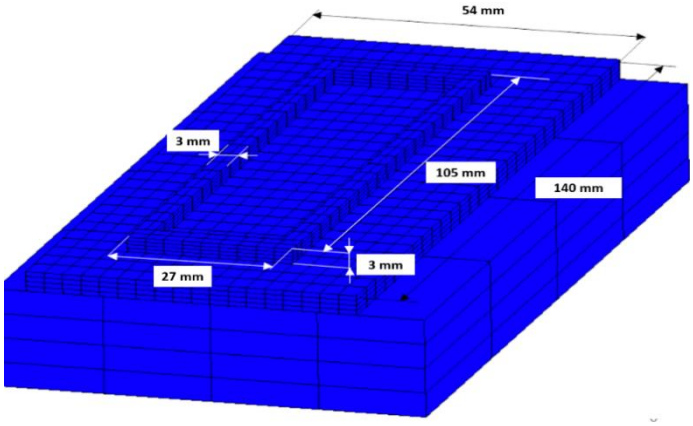


**Figure 10.** Numerical WAAM model designed for mesh sensitivity analysis

The main comparison criteria was the temperature distribution for the duration of WAAM process in which the method was conducted by dividing a finer mesh on each body consisting of table, substrate and filler with the total number of elements from 1268 to 4608. The sensitivity analysis was executed using a batch file analysis in MSC Marc/Mentat by developing a user routine that was able to run multiple WAAM simulation with different meshes at once.

The mesh sensitivity graph comparison is displayed in Fig. 11. Table 6 displays the numerical value of mesh sizes for each number of elements involved as well as computational time.

**Table 6:** Mesh sensitivity analysis

| Element set | Table | Substrate | Filler | Total number of Elements | Wall Time (s) | Convergence ratio | Maximum Temperature (°C) |
|---|---|---|---|---|---|---|---|
| Set 1 | 8 | 800 | 122 | 930 | 135 | 0.006 | 1598.3 |
| Set 2 | 32 | 1012 | 104 | 1268 | 140 | 0.002 | 1304.5 |
| Set 3 | 64 | 2016 | 448 | 2528 | 144 | 0.001 | 1186.9 |
| Set 4 | 128 | 4032 | 448 | 4608 | 597 | 0.013 | 1181.1 |

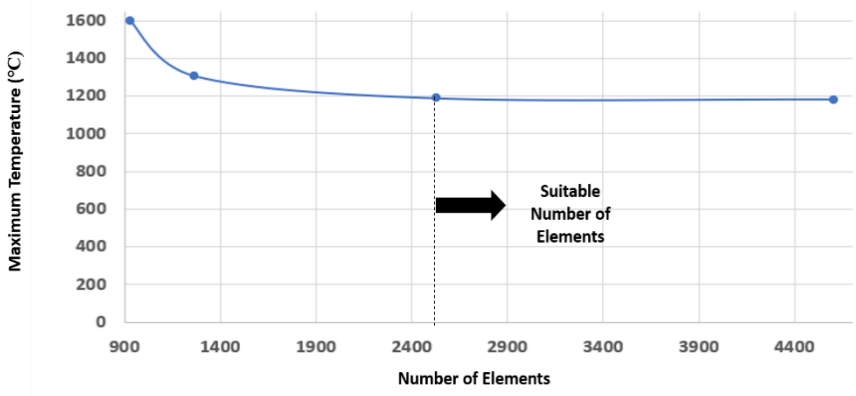


**Figure 11**: Mesh sensitivity analysis for maximum temperature

Based on Fig. 11 and Table 6, it can be observed that the final result of temperature was influenced by the number or the size of elements involved in the numerical computation. After the total number element of 2528 that corresponded to an element size of 1mm, the maximum temperature value showed similar range with relatively higher convergence ratio. Therefore, this element number or size (1 mm) was chosen as it had a lower computational time compared to finer mesh sizes.

## 3.0 RESULT AND DISCUSSION

After all basic procedures were fulfilled, the experimental substrate distortion caused by the twenty-five layers of wire deposition was analysed by comparing the result produced by VM. The experimental and simulation results of WAAM can be seen in Fig. 12 based on five tracking points on the top of the substrate.

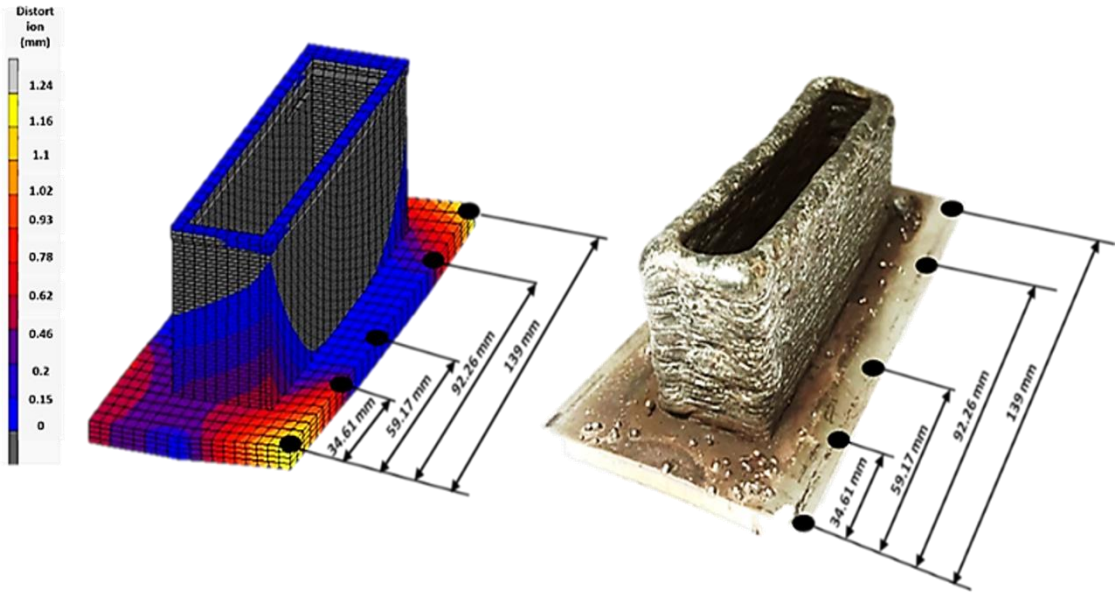


**Figure 12.** Location for distortion measurement at substrate of VM (left) and experiment (right)

As the benchmark of comparison, distortion of experimental process was the average value of five measurement points which were examined by utilizing the coordinate measurement machine (CMM) prior to and after the process. The exact identical locations were measured on post-processing stage in VM simulation and compared to the experimental distortion result. Table 7 exhibits the values of distortions which appeared in the substrate between experimental result and FE-based VM for both material modelling approaches along with their respective error percentage compared by means of average distortion. The graph visualization between VM and experiment is displayed in Fig. 13.

**Table 7:** Distortion results of experiment and virtual manufacturing

| | Distance (point of measurement) in mm | | | | | Average total distortion [mm] | Relative error percentage of total distortion [%] |
|---|---|---|---|---|---|---|---|
| | 0 | 34.61 | 59.17 | 92.26 | 139 | | |
| Experimental [mm] | 1.366 | 0.95 | 0.587 | 0.231 | 0.683 | 0.76 | - |
| FE-based VM with database material [mm] | 0.91 | 0.68 | 0.62 | 0.42 | 0.36 | 0.59 | 22.1 |
| FE-based VM Simulation with evolved component material [mm] | 1.14 | 0.857 | 0.411 | 0.198 | 0.784 | 0.68 | 11.1 |

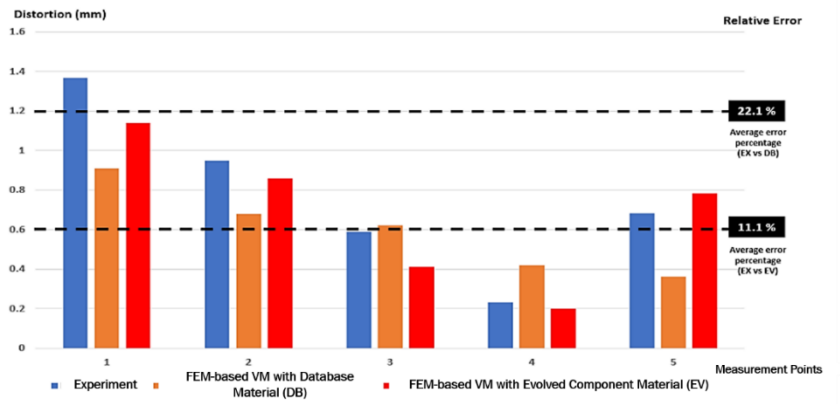


**Figure 13.** Results comparison between virtual manufacturing and experiment

From the distortion result displayed in Fig. 13 above, the distortion induced by WAAM process modelled by real component material had closer values compared to the experimental WAAM distortion while the distortion generated by WAAM simulation with database material had an overall much lower range compared to the component SS316L WAAM. This can be caused by the properties assigned within the component material in the VM simulation, which had more realistic resemblance with the actual SS316L material that was assigned during WAAM experimental process. The error percentage of the VM simulation using component material was 1% while VM simulation using database material had a larger error percentage of 22%.

## 4.0 CONCLUSION

The main objective of this research is to develop a basic procedure of VM which can be used as a guideline to predict geometrical distortion of final components. To verify the VM procedure, a series of experiment in the form of thin wall structure is carried out by using a pulsed GMAW process which considers the specific parameter settings controlled in the inverter and synergic power source. All parameters, dimensions and boundary conditions are set in a similar manner to ensure the realistic comparison in both studies. As a final conclusion, the following contributions can be summarized:

1. A practical procedure of FE-based VM for twenty-five layers deposition of WAAM on top of thin plate had been successfully executed based on actual experimental results which were conducted using two different material modelling approaches namely database and actual component SS316L.
2. The simplified bead model with rectangular mesh form allows the reduction of pre-processing and computational time. For this welding parameters, hexahedral mesh elements with average thickness are designed.
3. The well-known Goldak's double ellipsoid heat source model can be improved for rectangular mesh geometry to simulate temperature distribution.
4. The thermal calibration analysis shows similar temperature distribution pattern between WAAM simulation and experiment by adjusting the major heat transfer coefficients.
5. A mesh sensitivity analysis is of importance and should be conducted prior to final numerical simulation. It was decided to use numerical model with 2528 total number of elements due to constant maximum temperature value and an ideal computational time.
6. The substrate distortion results display the error percentage of VM with database material as 22.1% while the VM simulation using real SS316L component has a smaller error percentage (11.1%) when compared to WAAM experiment.
7. The difference in the temperature and substrate distortion result might be due to material inhomogeneity, parameters fluctuations, robotic system inconsistency etc.
8. This procedure is not the final one but it can be enhanced with additional stages for more advanced research.

As for further recommendation, it is proposed that the direct usage of "Component with Substrate" is to be planned such as investigation on rectangular heat source model, plastic strain etc.

## ACKNOWLEDGEMENT

The authors would like to express their gratitude to staff members of Smart Manufacturing Research Institute (SMRI) as well as staff of Welding Laboratory, Advanced Manufacturing Laboratory, Advanced Manufacturing Technology Excellence Centre (AMTEx) and Research Interest Group: Advanced Manufacturing Technology (RIG:AMT) at the Faculty of Mechanical Engineering, Universiti Teknologi MARA (UiTM) as well as Professorship of Virtual Production Engineering at Chemnitz University of Technology (CUT) in Germany for encouraging this research where simulation was partially carried out. This research is supported by DAAD Germany with Project Code: 57525437 (Future Technology Additive Manufacturing).

## REFERENCES

[1] Q. Wang, "Virtual manufacturing and systems" *E Manufacturing*.; 2005. DOI:10.2495/978-1-85312-998-8/09

[2] V.G Bharath, R. Patil, "Virtual Manufacturing: A Review" *International Journal of Engineering Research and Technology: NCRERAME 2015 Conference Proceeeding*., vol 3, no 17, 2015, DOI:10.1015/j.NCRERAME.2015.10.017

[3] C. Shukla, M. Vazques *et al*., "Virtual manufacturing: an overview," *Computer India Engineering*. Vol 31, pp. 79-82, 1996 DOI:10.1016/0360-8352(96)00083-6

[4] K. Iwata et al., "Modelling and Simulation Architecture for Virtual Manufacturing Systems" *CIRP Ann - Manuf Technol*. vol 44, no 1, pp. 399-402, 1995. DOI:10.1016/S0007-8506(07)62350-6

[5] H.G Lemu, "Virtual engineering in design and manufacturing," *Additive Manufacturing*, vol 2, no 4, pp. 289-294, 2014. DOI:10.1007/s40436-014-0085-y

[6] F. Klocke and A. Straube, "Virtual Process Engineering – An approach to integrate VR, FEM, and

simulation tools in the manufacturing chain,", 2004;5. DOI:10.1051/meca:2004021

[7] Li, Y. Sun et al., "Enhanced beads overlapping model for wire and arc additive manufacturing of multi-layer multi-bead metallic parts," J *Mater Process Technol*, vol 242, pp. 838-848, 2018, DOI:10.1016/j.jmatprotec.2017.10.017

[8] J. Xiong, R. Li et al., "Heat propagation of circular thin-walled parts fabricated in additive manufacturing using gas metal arc welding. *J Mater Process Technol.* 2018;251(August 2017):12-19. vol 251, pp. 12-19, 2018. DOI:10.1016/j.jmatprotec.2017.08.007

[9] K. Derekar, J. Lawrence et al., "Influence of Interpass Temperature on Wire Arc Additive Manufacturing (WAAM) of Aluminium Alloy Components," *MATEC Web of Conference*, vol 269, 2019. DOI:10.1051/matecconf/201926905001.

[10] ER. Delinger, P. Michaleris, "Effect of stress relaxation on distortion in additive manufacturing process modeling," *Additive Manufacturing* vol 12, pp. 51-59, 2016. DOI:10.1016/j.addma.2016.06.011

[11] C. Cambon, I. Bendaoud, S. Rouquette et al., "Influence of the first weld bead on strain and stress states in wire + arc additive manufacturing," *HAL Id* : hal-01954354. 2018.

[12] F. Montevecchi, G. Venturini et al., "Finite Element Modelling of Wire-arc-additive-manufacturing Process," *Procedia CIRP*. vol 55, pp. 109-114, 2016. DOI:10.1016/j.procir.2016.08.024

[13] M. Graf, A. Hälsig et al., "Thermo-mechanical modelling of wire-arc additive manufacturing (WAAM) of semi-finished products," *Metals (Basel)*, vol 8, no 12, 2018. DOI:10.3390/met8121009

[14] Y. Yehorov, L.J Da Silva, A. Scotti, "Exploring the use of switchback for mitigating homoepitaxial unidirectional grain growth and porosity in WAAM of aluminium alloys," *Int J Adv Manuf Technol*. vol 104, no 1-4, pp. 1581-1592, 2019. DOI:10.1007/s00170-019-03959-w

[15] T. He, S. Yu et al., "High-accuracy and high-performance WAAM propeller manufacture by cylindrical surface slicing method", *Int J Adv Manuf Technol*. vol 105, 2019. DOI:10.1007/s00170-019-04558-5

[16] B. Panda, K. Shankhwar et al., "Evaluation of genetic programming-based models for simulating bead dimensions in wire and arc additive manufacturing," *J. Intell Manuf*. November 2016. DOI:10.1007/s10845-016-1282-2

[17] Z. Hu, X. Qin et al., "Multi-bead overlapping model with varying cross-section profile for robotic GMAW-based additive manufacturing", *J Intell Manuf*. October 2019. DOI:10.1007/s10845-019-01501-z

[18] S. M, Rai S., Kumar et al. "Temperature distribution and residual stresses due to multipass welding in type 304 stainless steel and low carbon steel weld pads," *Int J Press Vessel*, vol 78, pp. 308-317, 2001. DOI:10.1016/S0308-0161(01)00047-3

[19] I. Tolosa, F. Garciandía et al., "Study of mechanical properties of AISI 316 stainless steel processed by "selective laser melting", following different manufacturing strategies," *Int J Adv Manuf Technol*. vol 51, pp. 639-647, 2010. DOI:10.1007/s00170-010-2631-5

[20] P. Li, Y. Gong et al., "Effect of post-heat treatment on residual stress and tensile strength of hybrid additive and subtractive manufacturing," *Int J Adv Manuf Technol*. vol 103, 2019. DOI:10.1007/s00170-019-03705-2

[21] K. D Ramkumar et al., "Characterization of metallurgical and mechanical properties on the multi-pass welding of Inconel 625 and AISI 316L," *J Mech Sci Technol*. vol 29, 2014. DOI:10.1007/s12206-014-1112-4

[22] N. Haneklaus, C. Cionea et al., "Hybrid friction diffusion bonding of 316L stainless steel tube-to-tube sheet joints for coil-wound heat exchangers," *J Mech Sci Technol*. vol 30, pp 4925-4930, 2014. DOI:10.1007/s12206-016-0832-z

[23] Y.H.P Manurung, K.P Prajadhiana et al., "Anaysis of material property models on WAAM distortion using non-linear numerical computation and experiment verification with P-GMAW", *Archives of Civil and Mechanical Engineering*. vol 21, 2021. DOI: 10.1007/S43452-021-00189-4

[24] K.P Prajadhiana, Y.H.P Manurung et al., "Development of bead modelling for distortion induced by wire arc additive manufacturing," *Matec Web of Conferences*. vol 269, 2019. DOI: 10.1051/matecconf/201926905003

[25] J. Guo et al., "Thomson RC. Influence of weld thermal cycle and post weld heat treatment on the microstructure of MarBN steel," *Int J Press Vessel Pip*. vol 174, pp. 13-24, 2019. DOI:10.1016/j.ijpvp.2019.05.010

[26] N. Saunders, G. Zhanli et al., "Using JMatPro to model material properties and behavior," *JOM: The Journal of the Minerals, Metals and Material Society*. vol 55, no 12, pp. 60-65, 2003 doi: 10.1007/s11837-003-0013-2

[27] M. Hamahmy, I. Deiab, "Review and analysis of heat source models for additive manufacturing", *Int J Adv Manuf Technol*. 2019. DOI:10.1007/s00170-019-04371-0

[28] D.H Ang, C.H Kim et al., "Numerical analysis of welding residual stress using heat source models for the multi-pass weldment", *KSME Int J*. vol 16, pp. 1054-1064, 2002.

[29] M. Abid, M.J Qarni, "3D thermal finite element analysis of single pass girth welded low carbon steel pipe-

flange joints," *Turkish Journal of Engineering and Enviromental Science*. vol 33, pp. 281-293, 2009. doi 10.3906/muh-0912-6.

[30] J. Zhang, L. Yu et al., "Effect of welding sequences on the welding stress and distortion in the CFETR vacuum vessel assembly using finite element simulation," *Int J Press Vessel* Pip. vol 175(July), 2019. DOI:10.1016/j.ijpvp.2019.103930.

[31] T.S Kumar, N. Atikukke, R. Kannan, "Thermal cycling effects on the creep-fatigue interaction in type 316LN austenitic stainless steel weld joint", *Int J Press Vessel Pip*. 2019:104009. DOI:10.1016/j.ijpvp.2019.104009.

[32] D.V Duvaraj, "3D Finite element simulation of temperature distribution, residual stresses on 304 stainless steel plates using GTA welding, "*Journal of Mechanical Science and Technology*. vol 30, pp. 67-76, 2017. DOI:10.1007/s12206-015-1208-5.

[33] Z. Hu, X. Qin, T. Shao, "Welding Thermal Simulation and Metallurgical Characteristics Analysis in WAAM for 5CrNiMo Hot Forging Die Remanufacturing," *Procedia Eng*. vol 207, pp. 2203-2208, 2017. DOI:10.1016/j.proeng.2017.10.982

[34] L. Guo, J. Xiang, "A numerical investigation of mesh sensitivity for a new three-dimenstional fracture model within the combined finite-discrete element method," *Engineering Fracture Mechanics*. vol 151, 2017. DOI: 10.1016/j.engfracmech.2015.11.006